(Received 20 March 2024, Accepted 27 May 2024, Scheduled 13 June 2024)

A Metasurface-Based Low-Profile Circularly Polarized Antenna with Double-Wide Beam for Global Navigation Satellite System

Ao Ni[1], Wen Wang[2], Jincheng Xue[2], Zhuopeng Wang[2], and Lili Zhang[2,*]

[1] College of Ocean Science and Engineering, Shandong University of Science and Technology, China
[2] College of Electronic and Information Engineering, Shandong University of Science and Technology, China

ABSTRACT: This study introduces a metasurface-based low-profile circularly polarized (CP) antenna with double-wide beam for global navigation satellite systems (GNSSs), which covers primarily BDS-2 B1 band and BDS-3 B1 band. At first, a T-slot structure achieving a compact design is presented to effectively miniaturize the antenna. Except that, a gear-type parasitic ring and eight parasitic microstrip lines are proposed to broaden both the half power beamwidth (HPBW) and axial ratio beamwidth (ARBW) of the antenna. Furthermore, a metasurface unit featuring double "WIFI" logo structure is introduced. This unit is expanded into a $7 * 7$ metasurface loaded under the antenna, significantly improving its radiation characteristics. After experimentation, the proposed antenna achieves notable results: 121° HPBW and 214° 3 dB-ARBW at 1.561 GHz and 121° HPBW and 236° 3 dB-ARBW at 1.575 GHz. Additionally, it demonstrates more than 3.52 dBic gain across the whole frequency band, whose simulation and test results are in agreement. These results show that the antenna can be used for various satellite communication systems necessitating CP antennas with wide ARBW and HPBW.

1. INTRODUCTION

The study of CP antenna bandwidth and beamwidth has significant importance in satellite system field. Beamwidth in CP antennas is characterized by two aspects: the Half Power Beamwidth (HPBW) concerning power distribution and the 3 dB Axial Ratio Beamwidth (ARBW) related to polarization angles. CP antennas find widespread application in satellite communications and Global Navigation Satellite Systems (GNSSs) [1] to mitigate polarization mismatches, suppress multipath effects, and counter Faraday rotation. As communication satellites are not always positioned directly overhead, the necessity for wide-beam CP antennas arises to cover a broad spatial angular range. Therefore, enhancing the beamwidth of CP antennas is crucial and offers substantial practical value in ensuring comprehensive coverage in satellite communication systems and GNSS applications.

CP microstrip antennas have been widely used in many communication systems, such as satellite communication systems, telemetry and remote control systems, and mobile communication systems, due to their low profile, low cost, and adaptability to mounting structures. However, the beamwidth of conventional patch antennas is usually about 70°–100°, which is too narrow to meet the system requirements [2]. Some approaches, such as using high permeability substrates [3], employing folded structures [4–6], or operating higher patterns [7, 8], have been reported to improve the performance. As for broadening the HPBW of antenna in dual bands, a metal pin shorting ground excitation [9] or a pair of dipoles [10] is used to excite the high secondary mode, which achieves dual bands by a parasitic metal structure and ensuring 3 dB ARBW beyond 120°. However, the height of this antenna is more than 21 mm, and the antenna profile is high. A slotted helical antenna [11] operating in Global Positioning System (GPS) L1 and L2 bands was designed with a sequential rotation technique to achieve an HPBW of 132° and 97° and an ARBW of 100° on the dual bands, respectively, but the profile height of the antenna exceeded 0.35λ. A right circularly polarized (RHCP) dual-band quadruple inverted F/L antenna (QIFLA) for GPS L1/L2 band [12] was proposed to achieve an HPBW of more than 120° and also an ARBW of 120° and 90°, respectively, using four spiral-shaped dual-band antennas. As for miniaturizing the antenna, a compact design featured modified dipoles forming four cross-symmetric sector arms and a magnetoelectric dipole [13], extending the ARBW to more than 130° while maintaining a low profile (0.054λ), but with a smaller HPBW. In recent years, much attention has been paid to increasing the beamwidth of CP antennas and designing a compact structure using metasurface structures, which are often used as coverings, reflectors, or radiating elements. In [14], a low-profile wide-beam CP antenna was designed in which metasurface was used as a radiating element to achieve an ARBW of more than 205°.

In this paper, a dual wide-beam navigation antenna based on metasurface is proposed. By loading the proposed T-slot, a parasitic structure and metasurface with $7 * 7$ dual "WIFI" logo-type structure, the antenna exhibits improved gain and beamwidth, delivering exceptional performance. Section 2 provides the detailed structure of the proposed antenna and design process. Section 3 focuses on the design of the metasurface with a dual "WIFI" logo-type structure, while Section 4 presents the performance results of the proposed antenna. Furthermore, a prototype was fabricated and measured in Section 5 to demonstrate the effectiveness of the design. A comparison

* Corresponding author: Lili Zhang (zhanglili@sdust.edu.cn).

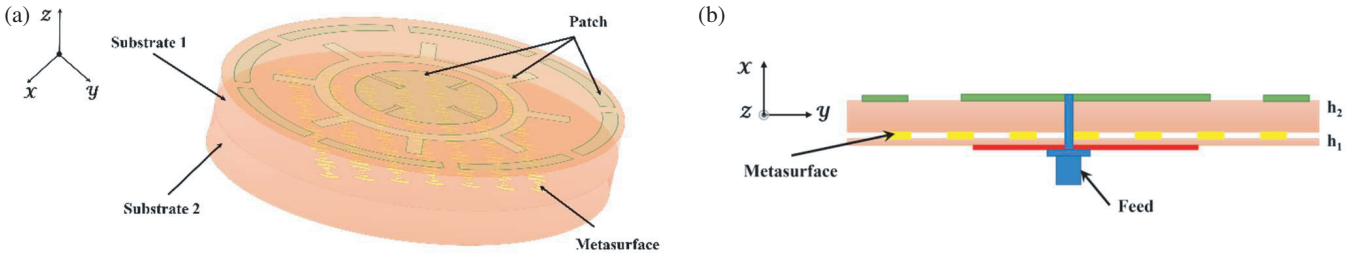

FIGURE 1. Structure of the proposed loaded antenna. (a) 3D model view. (b) Cross-sectional view.

TABLE 1. Dimensions of the proposed antenna.

Parameters	R	l	L_1	W_1	L_2	W_2	L_3	W_3	k
Size (mm)	5	1	11	1	8	1	10	2	2.2
Parameters	R_1	R_2	R_3	R_4	p	r	$r1$	s	$feed_y$
Size (mm)	23.9	27	45	30	8	0.4	1.1	0.8	9

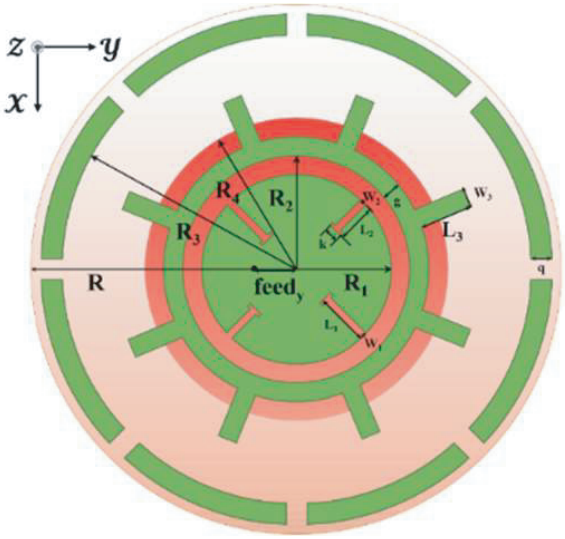

FIGURE 2. Structure diagram of the navigation antenna.

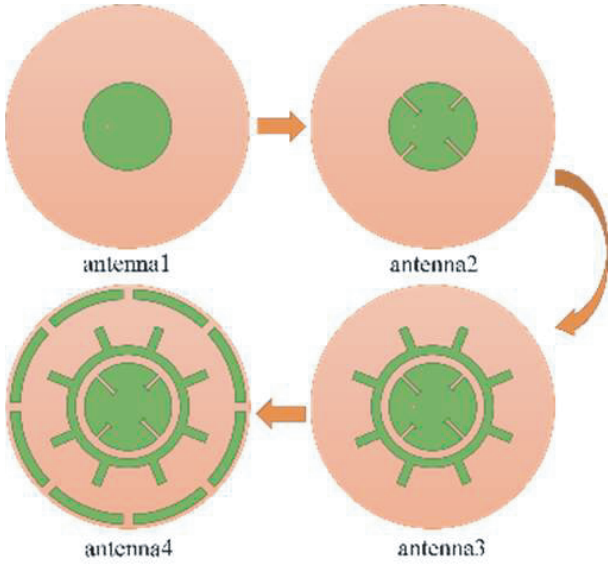

FIGURE 3. The design process of the navigation antenna.

between this design and some previous navigation antennas is also presented, followed by conclusions in Section 6. In particular, the proposed navigation antenna has a good performance with a low profile and a wide beam.

2. ANTENNA STRUCTURE AND DESIGN PROCEDURE

The proposed metasurface based dual wide beam navigation antenna is composed of 7∗7 double "WIFI" logo type metasurface units as the reflector of the dual wide beam navigation antenna to improve the gain and ARBW as shown in Figure 1. The height of the antenna is 4 mm, and the specific dimensions of the antennas are shown in Table 1. The structure of the whole antenna consists of two dielectric substrates. Dielectric substrate 1 is printed for the double wide beam navigation antenna, which is recorded as the original antenna; dielectric substrate 2 is printed for the metasurface structure, which is combined with the original antenna to form the final proposed antenna, which is recorded as the loaded antenna. In the following subsections, they will be introduced in detail, respectively.

2.1. Original Navigation Antenna Design

The structure of the navigation antenna is shown in Fig. 2. The antenna is printed on an FR4 dielectric plate with $\varepsilon_r = 4.4$, $\tan\delta = 0.02$, and its radius is $R = 50$ mm, thickness $h_1 = 3$ mm. A circular patch is loaded on the upper surface of the dielectric plate, and the radius of the patch is R_1. Then, a T-slot structure is proposed, by loading T-slots of different lengths on the circular patch, introducing perturbation to achieve circular polarization, and the T-slot loading does not affect the radiation of the patch more but can change the current path to reduce the

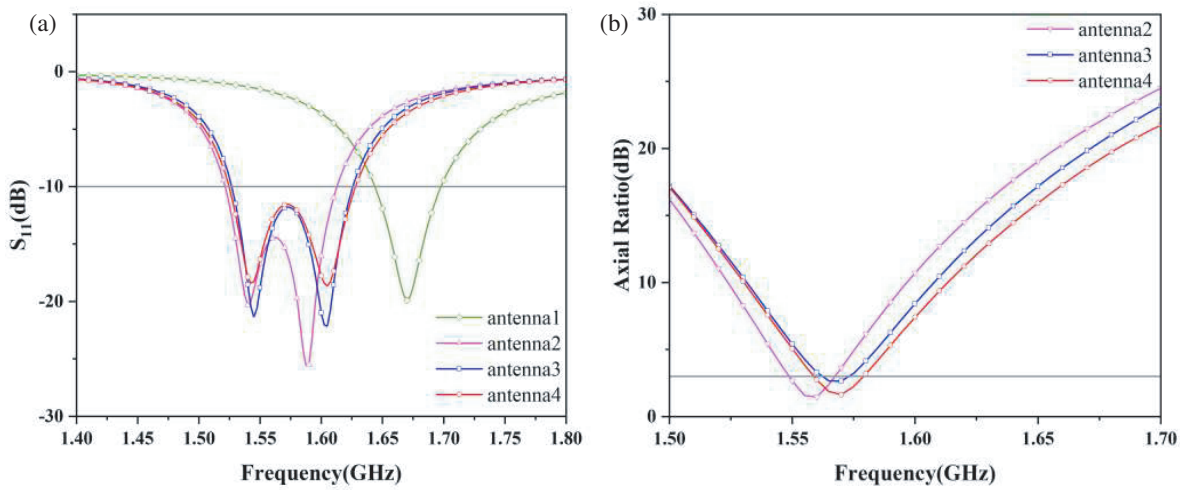

FIGURE 4. Performance of antennas with different configurations. (a) S_{11}. (b) Axial ratio bandwidth.

size of the patch and realize the design of antenna miniaturization. In addition, a gear-type parasitic structure is proposed to be loaded on the periphery of the circular patch, and finally eight curved microstrip lines are loaded in a circle around the radiating patch. Curved microstrip lines loaded around the circular radiating patch work like eight guides, which will cause part of the electromagnetic energy to be radiated to the side of the antenna, thus widening the HPBW and ARBW of the antenna. The lower surface of the dielectric substrate is a metal ground, and the radius of the dielectric substrate is R_4, $R > R_4$. Using the technique of dielectric substrate extension, most of the energy in the dielectric edge area radiates out along the normal direction, and part of it radiates in the tangential direction. The two parts of energy are superimposed in the far field, which widens the beam and finally realizes the double wide beam navigation antenna design.

The design process of the antenna is shown in Fig. 3. Antenna 1 consists of a circular patch; antenna 2 is loaded with two sets of T-slot structures of different sizes on the patch to form an asymmetric structure; antenna 3 is loaded with a geared parasitic structure at the periphery of the circular patch, and antenna 4 is loaded with eight curved parasitic strips at the outermost part of the dielectric substrate in a circular shape to form the final design.

2.2. Performance of the Original Navigation Antenna

The impedance matching bandwidth and axial ratio (AR) bandwidth of antennas with different structures are shown in Fig. 4. It can be seen that the matching bandwidth of antenna 1 is 1.64–1.70 GHz, and the radiation is linearly polarized. Antenna 2 is loaded with a T-shaped slit on the basis of antenna 1, and the resonant frequency of the antenna is reduced to achieve a miniaturized design and CP in the frequency band of 1.55–1.57 GHz. Antenna 3 has the same impedance matching bandwidth by adding the proposed gear-shaped parasitic ring at the periphery of the patch, but the AR bandwidth is moved to high frequency, and the bandwidth is reduced. Eight ring-shaped parasitic metal arcs are loaded at the periphery of the dielectric substrate of antenna 3 to form antenna 4, whose S_{11} bandwidth is basically unchanged, and the resonance is weakened, but the AR bandwidth is increased and reaches 1.56–1.58 GHz.

The simulated HPBW of antennas with different structures is shown in Fig. 5. It can be clearly seen from the figure that the HPBW of antenna 3 increases from 103° and 102° to 103° and 106° at the E and H planes at the low frequency point, respectively, by loading a gear-type parasitic structure; the HPBW of antenna 4 increases from 102° and 103° to 102° and 106° at the E and H planes at the high frequency point, respectively, and the increase is smaller; the gap parasitic structure of antenna 4, consisting of eight circular microstrip lines, enhances the lateral radiation energy of the antenna and increases the HPBW of the antenna to 140° and 143° in the xoz plane and yoz plane, respectively, at low frequency points, and 142° and 145° in the xoz plane and yoz plane, respectively, at high frequency points.

The 3 dB ARBW of the antennas at different stages are shown in Fig. 6. By comparison, it can be seen that the ARBW of antenna 3 increases from 135° to 184° at $\varphi = 0°$ at low frequencies and from 86° to 161° at high frequencies, but the ARBW decreases at $\varphi = 90°$. After antenna 4 is loaded with eight curved microstrip lines in a circle around the radiating patch, the ARBW at the low frequency point is increased from 184° and 100° at antenna 3 to 205° and 102° at $\varphi = 0°$ and $\varphi = 90°$; the ARBW at the high frequency point is increased from 161° and 122° at antenna 3 to 183° and 150° at $\varphi = 0°$ and $\varphi = 90°$, compared with antenna 2. In the plane of $\varphi = 0°$, the low frequency point and high frequency point at increased by 70° and 97° respectively.

It can be concluded that antenna 3 has improved the HPBW and ARBW of the antenna by adding the proposed gear-shaped parasitic ring at the periphery of the patch. Antenna 4 is loaded with eight ring-shaped parasitic metal strips at the outermost periphery of the dielectric substrate to form eight guides, which enhance the electromagnetic radiation at the side of the antenna and further widen the HPBW and ARBW of the antenna, realizing the design of a double-wide beam antenna.

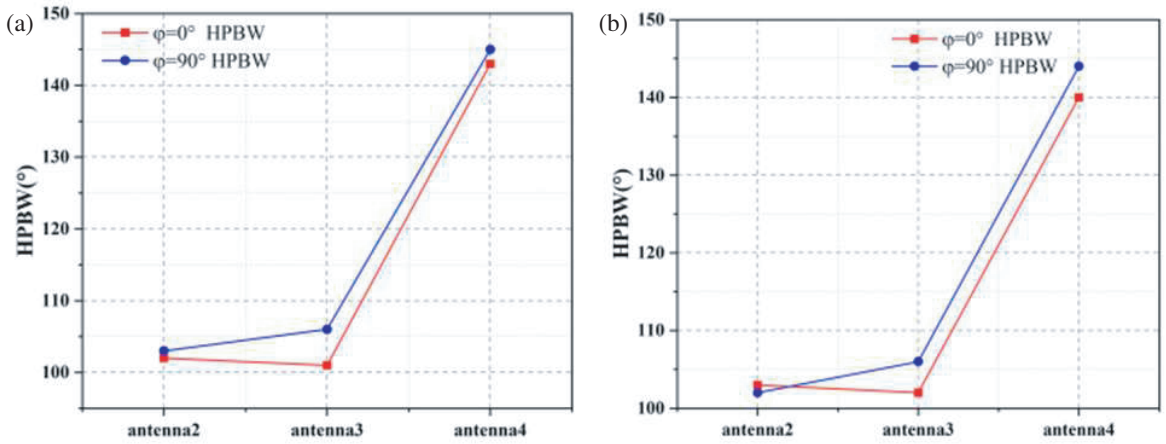

FIGURE 5. HPBW for different structured antennas. (a) 1.561 GHz. (b) 1.575 GHz.

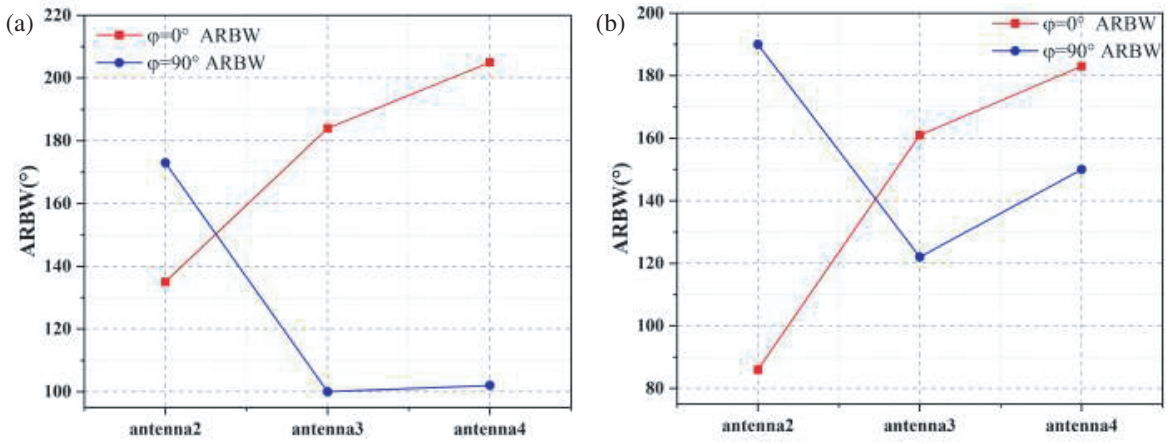

FIGURE 6. ARBW for different structured antennas. (a) 1.561 GHz. (b) 1.575 GHz.

2.3. Metasurface Structure Design

The antenna designed in Subsection 3.2 can achieve a wider beamwidth and axial ratio beamwidth in the frequency band, but its gain is small, and a metasurface structure is proposed below to extend the beamwidth and improve the gain of the antenna.

In this section, a double "WIFI" logo type structure of double negative metasurface is proposed, which consists of a central circle and four peripheral arcs, named after the inverted symmetric WIFI logo pattern. The cell structure of the metasurface is shown in Fig. 7, and the metal patch of the double "WIFI" type metasurface cell structure is printed on the upper surface of the FR4 dielectric substrate with the thickness of $h_2 = 1$ mm. As shown in the figure, the spacing of the double "WIFI" type cell structure is p; the radius of the central circle is r_2; the radii of the peripheral branches are r_1 and r; their widths are n; and the spacing is n.

2.4. Research on the Principle of Gain Enhancement of Antenna by Metasurface

The general method used to increase the gain of the antenna is to make the antenna constitute a Fabry-Perot (F-P) resonant cavity structure, also known as F-P antenna, which is composed of two parts, including feed antenna and partial reflection surface, as in Fig. 8. This kind of reflective surface with partial reflection characteristics will cause the incident electromagnetic wave to be partially reflected and partially transmitted, rather than all reflections and transmissions [15]. When the partially reflective surface is at a certain height above the antenna, a resonant cavity structure is formed between the partially reflective surface and the reflective floor, and the electromagnetic wave radiated from the antenna repeatedly reflects and transmits partially through this resonant cavity structure. In case the separation between the two satisfies the corresponding resonance conditions, the transmitted electromagnetic waves will be superimposed in the same phase, so that the radiation capacity of the antenna can be improved.

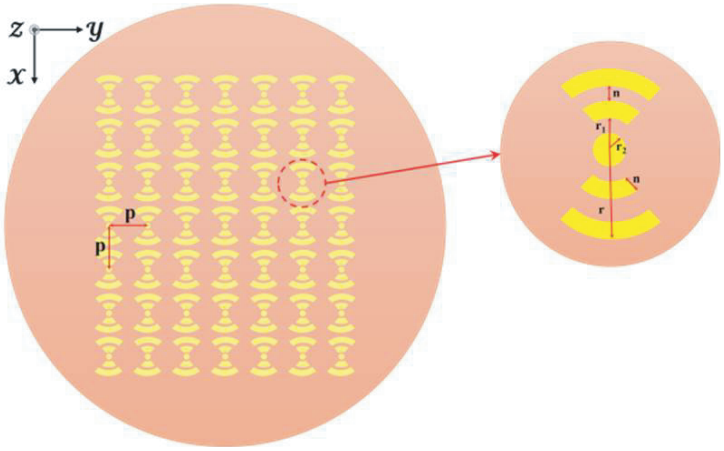

FIGURE 7. Double "WIFI" type metasurface structure.

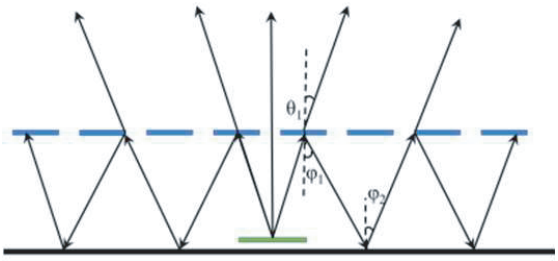

FIGURE 8. Illustration of the F-P antenna structure.

Suppose that φ_1 and θ are the reflected and transmitted phases of the frequency selective surface (FSS) above the antenna, respectively, that φ_2 is the reflected phase of the ground plane, that the reflection coefficient of the FSS is R, and that the transmission coefficient is T. Then the transmission coefficients are [16]:

$$r = \mathrm{R}e^{j\varphi_1} \tag{1}$$

$$t = \mathrm{T}e^{j\theta} \tag{2}$$

The transmission coefficient after direct transmission of electromagnetic waves can be expressed as:

$$t_0 = t \tag{3}$$

The propagation constant $k = 2\pi/\lambda$ in free space is known, and the electromagnetic wave transmission coefficient after one reflection can be expressed as:

$$t_1 = tre^{\frac{2jkh}{\cos\theta}+2jkh\tan\theta\sin\theta+j\varphi_2} = tre^{-2jkh\cos\theta+j\varphi_2} \tag{4}$$

It can be calculated that the transmission coefficient of the final transmitted wave of the electromagnetic wave after n reflections can be expressed as:

$$t_n = tr^n e^{-2jnkh\cos\theta+jn\varphi_2} \tag{5}$$

In summary, the sum of transmission wave transmission coefficients can be obtained as,

$$t_\alpha = \sum\nolimits_0^\infty t_n = \frac{t}{1-re^{-2jkh\cos\theta+j\varphi_2}} \tag{6}$$

Since $T^2+R^2=1$, the power transfer coefficient can be expressed as,

$$D = t_\alpha t_\alpha^* = \frac{1-R^2}{1-2R\cos\Phi+R^2} \tag{7}$$

where as [17],

$$\Phi = \frac{4\pi}{\lambda}h\cos\theta-\varphi_1-\varphi_2 \tag{8}$$

It can be seen that when $\cos\Phi = 1$ and $\theta = 0°$, i.e.,

$$\frac{4\pi}{\lambda}hc-\varphi_1-\varphi_2 = 2n\pi, \qquad n = 0,1,2\ldots \tag{9}$$

at this time:

$$f = \frac{c(\varphi_1+\varphi_2)}{4\pi h}-\frac{cn}{2h}, \qquad n = 0,1,2\ldots \tag{10}$$

D can be taken as the maximum value:

$$D = \frac{1-R^2}{1-2R+R^2} = \frac{1+R}{1-R} \tag{11}$$

As can be seen from the above equation, the greater the reflection coefficient of the resonant cavity antenna part of the reflective surface is, the greater the corresponding power transmission coefficient D is, the higher the antenna gain is, and the distance between the primary source and frequency selective surface action and resonance conditions are directly related.

In this paper, a single layer double "WIFI" type metasurface is loaded under the designed navigation antenna to improve the gain of the antenna and further optimize the ARBW of the antenna through the reasonable placement of the metasurface and the reasonable arrangement of the cell structure.

3. PERFORMANCE OF LOADED METASURFACE NAVIGATION ANTENNA

The impedance matching performance of the loaded antenna is illustrated in Fig. 9, with the red and black lines indicating the S_{11} curves for the original and loaded antennas, respectively. From the figure, it can be clearly seen that the impedance matching bandwidth of the loaded antenna is 1.53 GHz–1.63 GHz, and the relative bandwidth is 6.3%. From the figure, it can be seen that the impedance matching of the original antenna in the whole working band range has been greatly improved after loading the metasurface structure.

The ARs of the loaded antenna and original antenna simulation are compared in Fig. 10, from which it can be seen that the

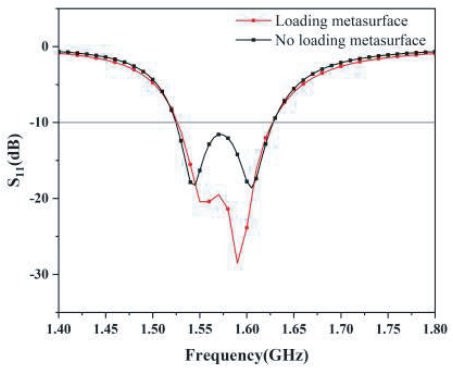

FIGURE 9. S_{11} of the original and loaded antennas.

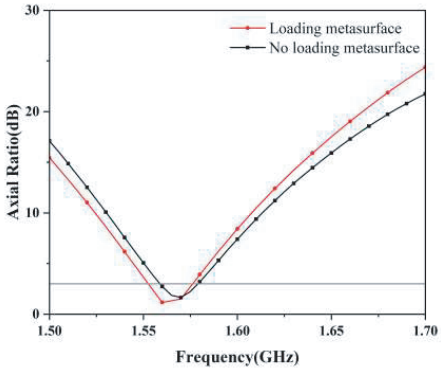

FIGURE 10. ARs of the original and loaded antennas.

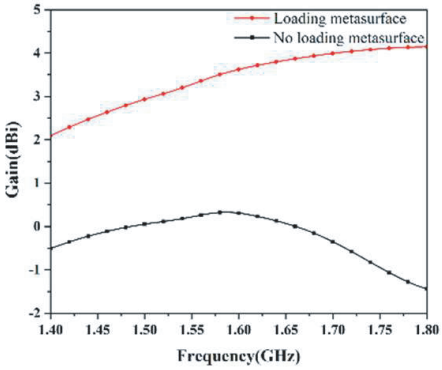

FIGURE 11. The gains of original and loaded antennas.

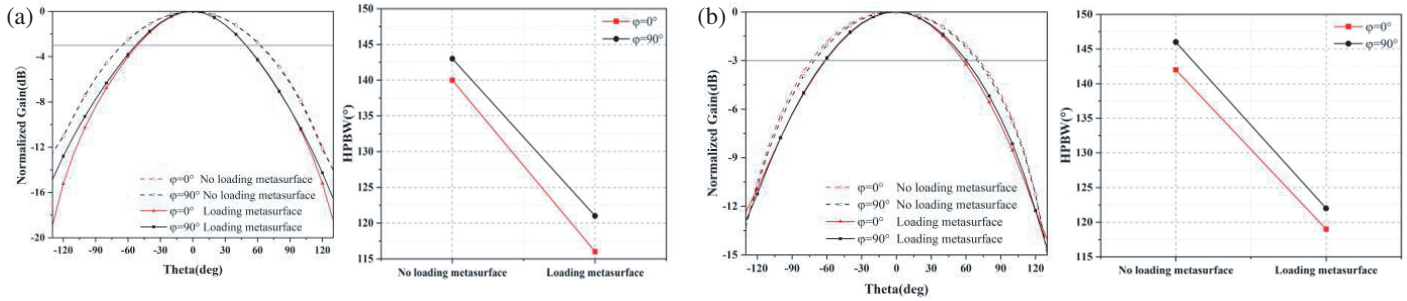

FIGURE 12. The HPBWs of the original and loaded antennas. (a) 1.561 GHz. (b) 1.575 GHz.

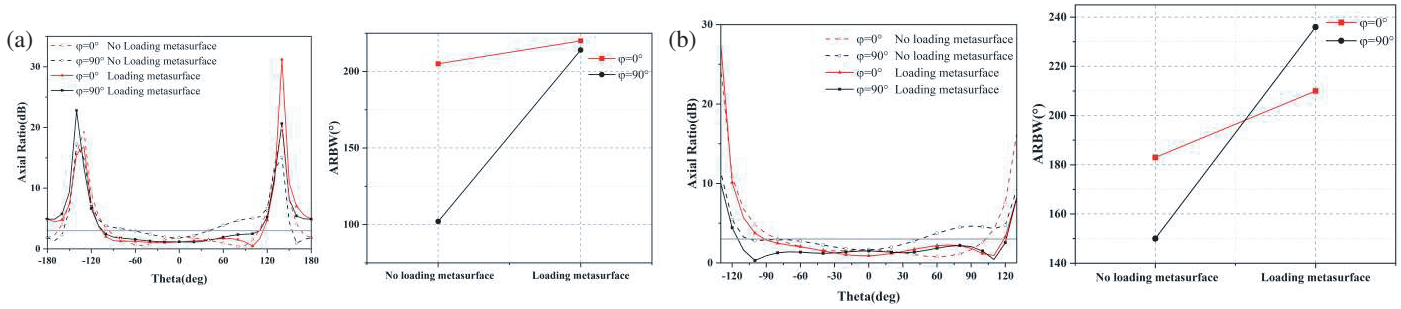

FIGURE 13. The ARBWs of the original and loaded antennas. (a) 1.561 GHz. (b) 1.575 GHz.

3 dB AR bandwidth of the loaded antenna is 1.55–1.58 GHz, and the relative bandwidth is 2%. Compared with the original antenna, the AR bandwidth and CP performance of the antenna are greatly improved after loading the metasurface.

As can be seen in Fig. 11, the maximum gain of the loaded antenna is 3.5 dBic in the whole working band, while the maximum gain of the original antenna is only 0.3 dBic in the working band, which shows that the overall gain of the original antenna has been improved after loading the metasurface.

The HPBWs of the loaded antenna at the BDS-2 B1 and BDS-3 B1 frequency points are shown in Figs. 12(a) and (b), respectively, from which it can be seen that the HPBWs at the BDS-2 B1 frequency points in the xoz and yoz planes are 116° and 121°, respectively, which is a decrease of 24° and 22° compared to the original antenna; the HPBWs at the B1 frequency point of BDS-3 is decreased from the original 143° and 146° to 117° and 121°, respectively. This is due to the loading of the metasurface, which makes the overall gain of the antenna improved, and according to the relationship between gain and beamwidth, it is known that the increase of gain must lead to the decrease of HPBW.

The 3 dB ARBWs at the BDS-2 B1 and BDS-3 B1 frequency points are shown in Figs. 13(a) and (b), respectively, from which it can be seen that the 3 dB ARBWs at the BDS-2 B1 fre-

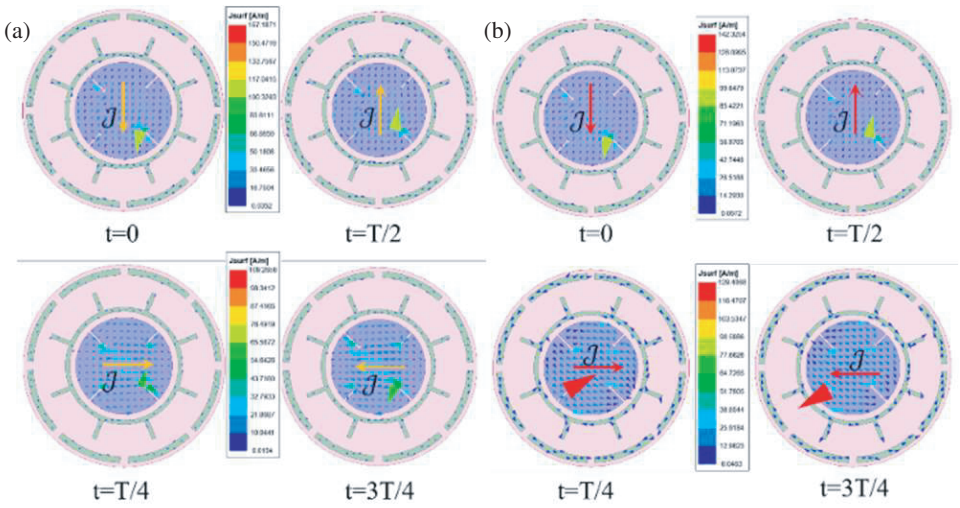

FIGURE 14. The current distribution of the loaded antenna. (a) 1.561 GHz. (b) 1.575 GHz.

quency points in the xoz and yoz planes are 220° and 214°, respectively, an increase of 15° and 112° compared to the original antenna; the ARBWs at the BDS-3 B1 frequency point change from the original 183° and 150° to 210° and 236°. Compared with the original antenna, the ARBW of the loaded antenna at the two frequency points is greatly improved after loading the metasurface, because it ensures that the two electric field components and amplitudes are almost equal in a wide angle, thus achieving a wide 3 dB ARBW.

The current distributions of the loaded antenna at BDS-2 B1 frequency point and BDS-3 B1 frequency point, respectively, are given in Fig. 14. Comparing the current distributions at different times $(0, 4/T, 2/T, 3/4T)$, it can be seen that the currents rotate in the counterclockwise direction, and thus RHCP radiation is obtained.

4. PARAMETER ANALYSIS

To further illustrate the design theory of the metasurface-based double-wide beam navigation antenna, this subsection investigates and analyzes the effects of the main parameters in the navigation antenna design on the antenna reflection coefficient, AR bandwidth, HPBW, and 3 dB ARBW. The parametric analysis is carried out on the basis of the metasurface based double-wide beam navigation antenna. According to the control variable method, only one parameter value is changed at a time during the analysis, and the rest of the parameter values are kept constant.

4.1. Changing the T-Slot Slit Length L_1 on the Antenna Performance

The variation of S_{11} and AR curves and the variation of HPBW and ARBW for the antenna with different L_1 values are given in Figs. 15(a), (b), (c), (d), (e), and (f), respectively. Under the condition of keeping other parameters constant, L_1 is taken as 10 mm, 11 mm, and 12 mm, respectively. It can be seen from the figure that as L_1 increases, the bandwidth of S_{11} gradually moves to lower frequencies; the bandwidth increases; and the resonance weakens. The axial ratio bandwidth also gradually moves to lower frequencies, and the axial ratio bandwidth increases; For HPBW, $\varphi = 0°$, at 1.561 GHz and 1.575 GHz HPBWs are gradually decreasing; in $\varphi = 90°$ plane, HPBWs at 1.561 GHz and 1.575 GHz are gradually increasing. For ARBW, because when $L_1 = 12$ mm, the antenna does not have 3 dB AR bandwidth, the ARBW under this is seen as 0°. In $\varphi = 0°$ plane, the ARBWs at 1.561 GHz and 1.575 GHz both increase first and then decrease; in $\varphi = 90°$ plane, the ARBWs at 1.561 GHz and 1.575 GHz both decrease gradually, according to the above analysis and the design index of the required antenna. Considering each performance of the antenna, $L_1 = 11$ mm is finally chosen.

4.2. Radius of the Arc r on the Antenna Performance

From the principle of metasurface design, it is known that the impedance bandwidth of the antenna will not be significantly affected after loading the metasurface at a suitable distance, and at the same time, the impedance matching level will be improved to some extent. Therefore, only the beamwidth of the antenna is analyzed.

The effects of the peripheral radius r on the HPBW and ARBW of the dual "WIFI" type metasurface unit structure are shown in Figs. 16(a), (b), (c), and (d), respectively. It can be seen from the figure, with the increase of r, when $\varphi = 0°$, the HPBWs at 1.561 GHz and 1.575 GHz are gradually reduced; for ARBW, in $\varphi = 0°$ plane, the maximum ARBW is obtained at $r = 3.5$ mm, which are 220° and 210° respectively; in $\varphi = 90°$ plane, the maximum ARBW is obtained at $r = 3.5$ mm, which are 214° and 236°, respectively. According to the above analysis, it can be seen that the value of r has a great influence on the ARBW of the antenna, and finally the radius of the peripheral arc $r = 3.5$ mm is chosen for the double "WIFI" logo type metasurface unit structure after comparing the performance.

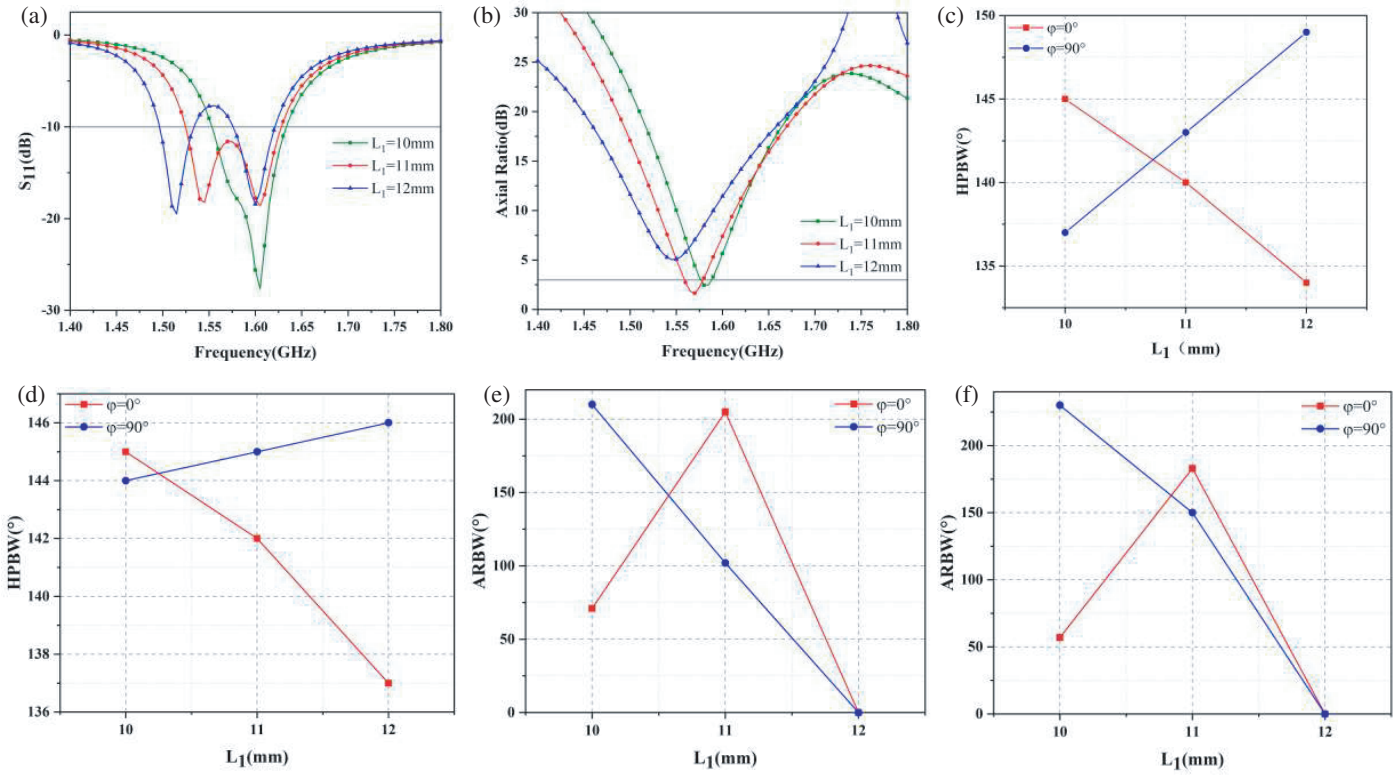

FIGURE 15. The performance of the antenna at different L_1 values. (a) S_{11}. (b) AR. (c) HPBW at 1.561 GHz. (d) HPBW at 1.575 GHz. (e) ARBW at 1.561 GHz. (f) ARBW at 1.575 GHz.

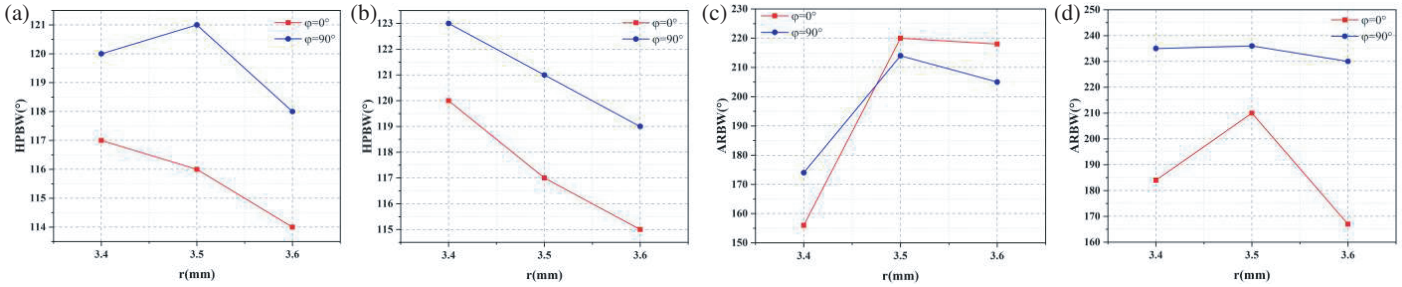

FIGURE 16. The performance of the antenna at different r values. (a) HPBW at 1.561 GHz. (b) HPBW at 1.575 GHz. (c) ARBW at 1.561 GHz. (d) ARBW at 1.575 GHz.

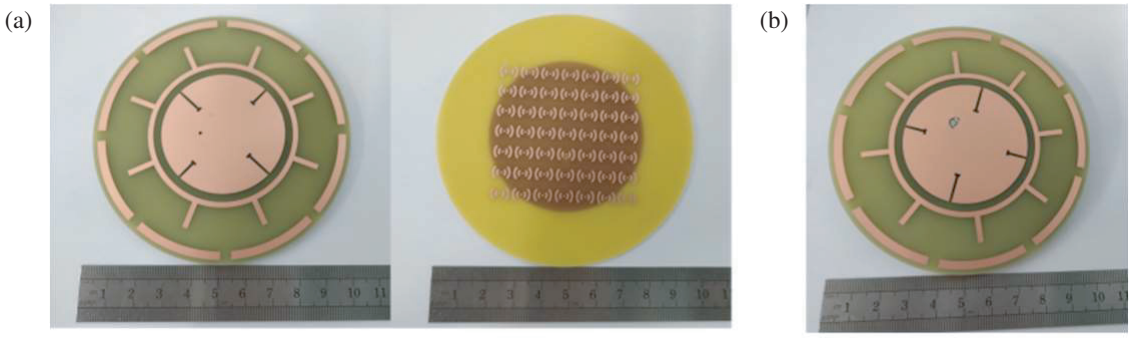

FIGURE 17. Fabrication of the antenna physical diagram. (a) Plan view. (b) Top view.

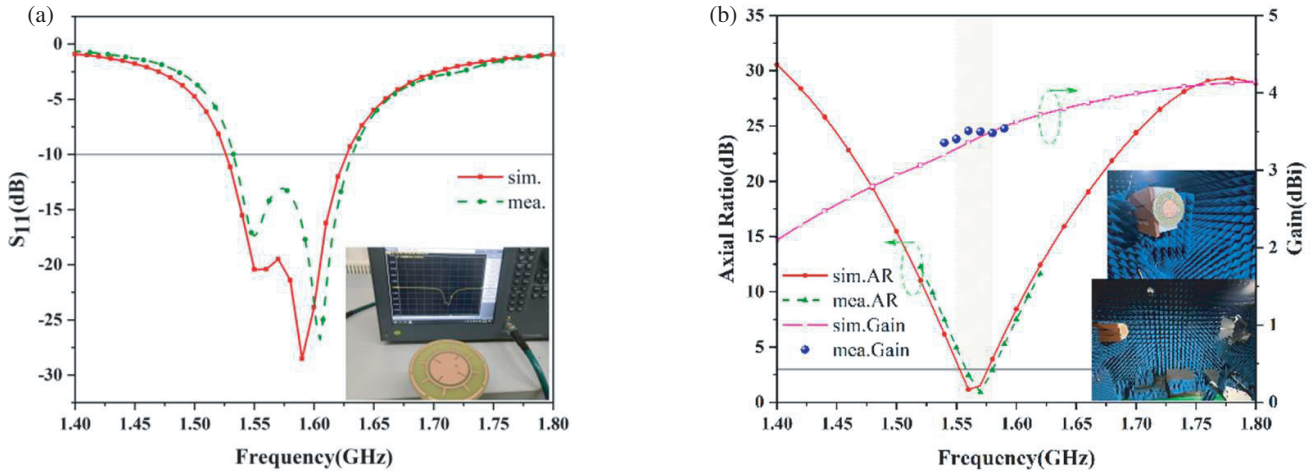

FIGURE 18. The S_{11} simulation and measurement results of the navigation antenna loaded with metasurface.

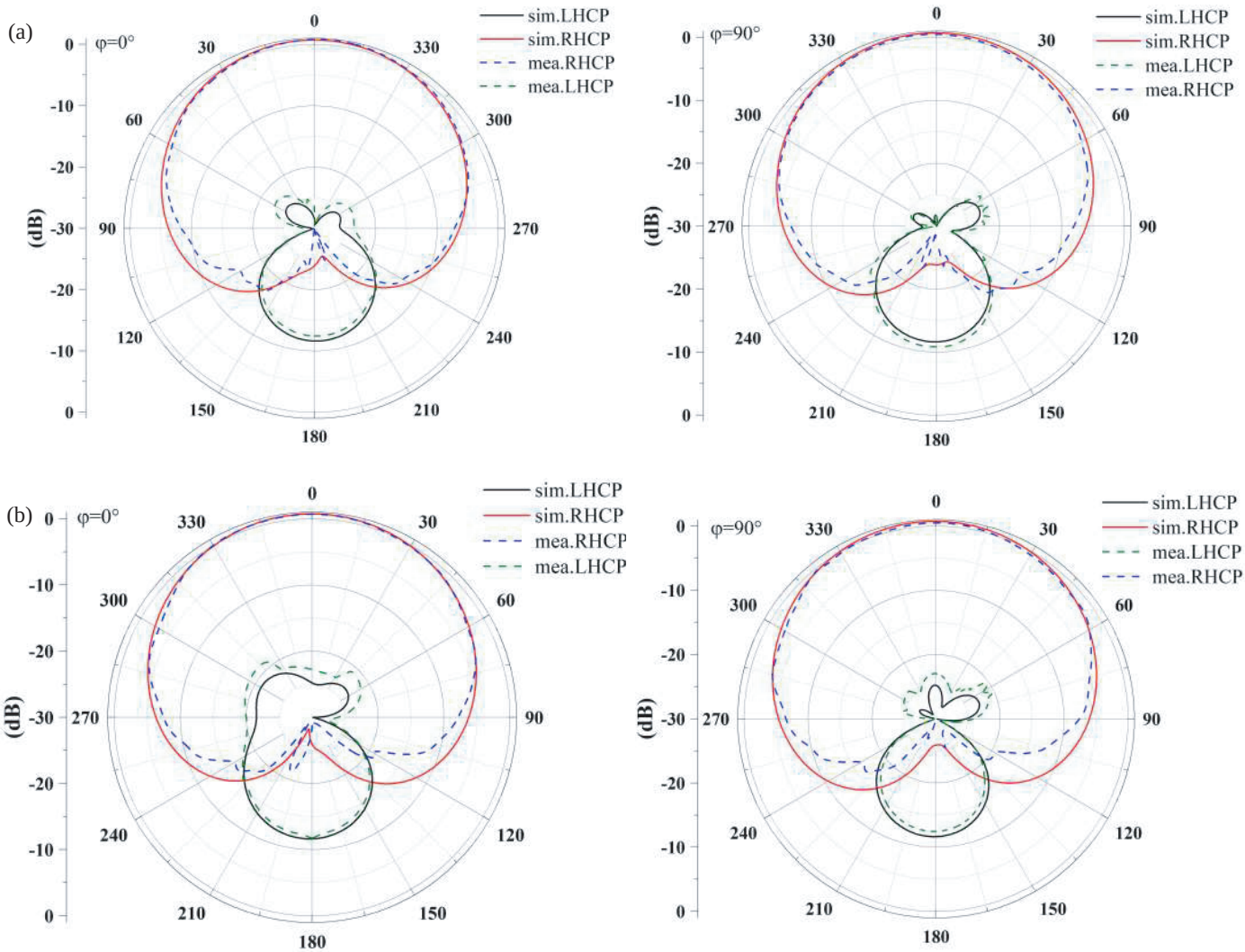

FIGURE 19. The radiation patterns simulation and measurement results of the navigation antenna loaded with metasurface. (a) 1.561 GHz. (b) 1.575 GHz.

TABLE 2. Comparison of the designed antenna with other antennas.

Ref.	Single- or dual-band	Overall size (mm^3)	Fre. (GHz)	HPBW / °		ARBW / °	
				$\varphi = 0°$	$\varphi = 90°$	$\varphi = 0°$	$\varphi = 90°$
[9]	Dual	$80 \times 80 \times 21.5$	1.256	122°	126°	123°	141°
			1.561	123°	129°	152°	212°
[10]	Dual	$80 \times 80 \times 12$	1.616	$< 120°$		$< 100°$	
			2.492				
[11]	Dual	$\pi \times 15 \times 15 \times 80$	1.575	132°	112°	$< 100°$	
			1.227	97°	95°		
[12]	Single	$39 \times 39 \times 6$	2.492	$< 100°$		135°	
						140°	
[13]	Dual	$35 \times 35 \times 10$	1.575	$> 120°$		120°	
						122°	
			1.227			90°	
						93°	
This Work	Dual	$\pi \times 50 \times 50 \times 4$	1.561	116°	121°	220°	214°
			1.575	117°	121°	210°	236°

5. FABRICATION AND EXPERIMENTAL RESULTS

In order to verify the correctness of the above theory, the designed antenna is fabricated as illustrated in Figure 17, and its dielectric substrate is FR4. The S_{11} test environment and the simulated and measured $|S_{11}|$ of the antenna are shown in Fig. 18(a), and it can be clearly seen from the figure that the measured $|S_{11}|$ bandwidth of the antenna is 1.53 GHz–1.63 GHz, compared with the simulated $|S_{11}|$ bandwidth 1.54–1.64 GHz, and the frequency band has a little shift, which may be due to the error caused by the fabrication and welding of the antenna, but the trend of the antenna's S_{11} simulated and measured curves is still relatively consistent.

The gain and AR of the antenna are given in Fig. 18(b), and it can be seen from the figure that the simulated AR bandwidth is 30 MHz (1.55 GHz–1.58 GHz); the relative bandwidth is 1.9%; the measured AR bandwidth is 29 MHz (1.558 GHz–1.587 GHz); the relative bandwidth is 1.8%; the simulated and tested curves are in good agreement. At the same time, it can also be seen that the simulated gain and measured gain of the antenna are in the same trend, both are greater than 3.5 dBic, and the average difference is smaller, about 0.3 dBic, which may be caused by the error introduced in the antenna processing.

The simulation and measurement results of the metasurface-based dual wide-beam navigation antenna with radiation pattern at 1.561 GHz and 1.575 GHz are given in Fig. 19. It can be seen from the figure that the antenna has good directional radiation performance at both frequency points, which meets the requirements of the navigation antenna. Overall, the measured radiation pattern of the antenna has a left hand circular polarization (LHCP) less than -20 dB, good right hand circular polarization (RHCP) and small back lobe, which can be applied to the required navigation system.

The antenna designed in this paper is shown in Table 2 for comparison with published antenna designs, and it can be seen that the antenna is able to achieve a wide HPBW and ARBW with good wide-beam characteristics at a relatively small size.

6. CONCLUSIONS

In this paper, a low-profile circularly polarized antenna with double wide-beams for a satellite navigation system based on metasurface is proposed. Not only is a T-slot structure presented to miniaturize the antenna, but also a gear-type parasitic ring is proposed to widen the HPBW and ARBW of the antenna. Besides, a dual "WIFI" logo-type structure of the metasurface unit is introduced, which is expanded to a $7 * 7$ metasurface loaded under the antenna to optimize its radiation characteristics. After measurement, it has a 121° HPBW and a 214° 3 dB-ARBW for BDS B1, as well as a 121° HPBW and a wider 236° 3 dB-ARBW for B3, specifically demonstrating its clear double wide-beam characteristics.

REFERENCES

[1] Abdul-Rahman, E. and D. N. Aloi, "Design of a multi-function global navigation satellite system and 5G cellular antenna structure for automotive applications using characteristic mode analysis," *IET Microwaves, Antennas & Propagation*, Vol. 17, No. 11, 863–871, 2023.

[2] Su, C.-W., S.-K. Huang, and C.-H. Lee, "CP microstrip antenna with wide beamwidth for GPS band application," *Electronics Letters*, Vol. 43, No. 20, 1062–1063, 2007.

[3] Pan, Z.-K., W.-X. Lin, and Q.-X. Chu, "Compact wide-beam circularly-polarized microstrip antenna with a parasitic ring for CNSS application," *IEEE Transactions on Antennas and Propagation*, Vol. 62, No. 5, 2847–2850, 2014.

[4] Elson, J. T., R. K. Butler, D. O. Reudink, and T. Achilles, "Planar antenna array with parasitic elements providing multiple beams of varying widths," Patent US6317100B1, 2001.

[5] He, H., "A novel wide beam circular polarization antenna-microstrip-dielectric antenna," in *2002 3rd International Con-*

ference on Microwave and Millimeter Wave Technology, 2002. Proceedings. ICMMT 2002., 381–384, IEEE, 2002.

[6] Ouyang, J., F. Yang, S. Yang, and Z. Nie, "A novel E-shape radiation pattern reconfigurable microstrip antenna for broadband, wide-beam, high-gain applications," *Microwave and Optical Technology Letters*, Vol. 50, No. 8, 2052–2054, 2008.

[7] Wang, S., Q. Zhu, X. Yun, and S. Xu, "Design of cylindrical conformal millimeter-wave microstrip antennas with broad beamwidth," *International Journal of Infrared and Millimeter Waves*, Vol. 28, 465–471, 2007.

[8] Li, C., F. Zhang, F. Zhang, F. Sun, and K. Yang, "A dual-band circularly polarized antenna with wide HPBWs for CNSS applications," *IEICE Electronics Express*, Vol. 15, No. 12, 20180409, 2018.

[9] Chen, K., J. Yuan, and X. Luo, "Compact dual-band dual circularly polarised annular-ring patch antenna for BeiDou navigation satellite system application," *IET Microwaves, Antennas & Propagation*, Vol. 11, No. 8, 1079–1085, 2017.

[10] Tran, H. H. and I. Park, "A dual-wideband circularly polarized antenna using an artificial magnetic conductor," *IEEE Antennas and Wireless Propagation Letters*, Vol. 15, 950–953, 2015.

[11] Yang, Y.-H., J.-L. Guo, B.-H. Sun, and Y.-H. Huang, "Dual-band slot helix antenna for global positioning satellite applications," *IEEE Transactions on Antennas and Propagation*, Vol. 64, No. 12, 5146–5152, 2016.

[12] Lin, J., Z. Qian, and W. Cao, "AMC-based planar antenna with low-profile and broad CP beamwidth," *IEICE Electronics Express*, Vol. 14, No. 15, 20170473, 2017.

[13] Liu, S., D. Yang, and J. Pan, "A low-profile circularly polarized metasurface antenna with wide axial-ratio beamwidth," *IEEE Antennas and Wireless Propagation Letters*, Vol. 18, No. 7, 1438–1442, 2019.

[14] Tae, H.-S., K.-S. Oh, W.-I. Son, W.-G. Lim, and J.-W. Yu, "Design of compact dual-band quadruple inverted-F/L antenna for GPS L1/L2 band," *IEEE Transactions on Antennas and Propagation*, Vol. 61, No. 4, 2276–2279, 2013.

[15] Ratni, B., W. A. Merzouk, A. d. Lustrac, S. Villers, G.-P. Piau, and S. N. Burokur, "Design of phase-modulated metasurfaces for beam steering in Fabry–Perot cavity antennas," *IEEE Antennas and Wireless Propagation Letters*, Vol. 16, 1401–1404, 2016.

[16] Ratni, B., W. A. Merzouk, A. d. Lustrac, S. Villers, G.-P. Piau, and S. N. Burokur, "Design of phase-modulated metasurfaces for beam steering in Fabry–Perot cavity antennas," *IEEE Antennas and Wireless Propagation Letters*, Vol. 16, 1401–1404, 2016.

[17] Trentini, G. V., "Partially reflecting sheet arrays," *IRE Transactions on Antennas and Propagation*, Vol. 4, No. 4, 666–671, 1956.